

Kinetic analysis and engineering of thermostable Cas12a for nucleic acid detection

Juan Pan ^{*}, Megumu Mabuchi, Daniel W. Kneller, Ryan T. Fuchs, Jennifer L. Curcuru, Esta Tamanaha, Nathan A. Tanner, G. Brett Robb , Ivan R. Corrêa, Jr. 

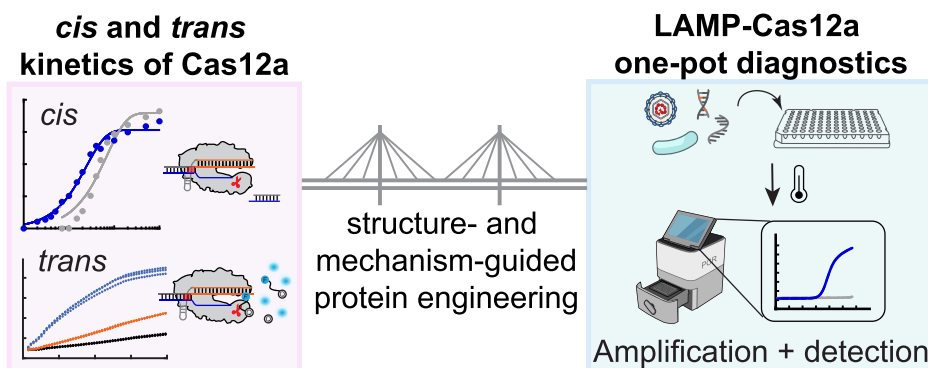
New England Biolabs Inc., Ipswich, MA 01938, United States

^{*}To whom correspondence should be addressed. Email: jpan@neb.com

Abstract

Cas12a *trans* nuclease activity has been leveraged for nucleic acid detection, often coupled with isothermal amplification to increase sensitivity. However, due to the lack of highly efficient thermostable Cas12a orthologs, use of Cas12a in one-pot combination with high temperature (55–65°C) amplification, such as loop-mediated isothermal amplification (LAMP), has remained challenging. Here, we attempt to address this challenge by comparative study of the thermostable, but poorly *trans*-active YmeCas12a (from Yellowstone metagenome) with the mesophilic, highly *trans*-active LbaCas12a (from *Lachnospiraceae* bacterium ND 2006). Kinetic characterizations identified that poor *trans* substrate affinity (high K_m) is the key limiting factor in YmeCas12a *trans* activity. We engineered YmeCas12a by structure-guided mutagenesis and fusion to DNA-binding domains to increase its affinity to the *trans* substrate. The most successful combinatorial variant showed 5–50-fold higher catalytic efficiency with the *trans* substrate depending on the target site. With the improved variant, we demonstrate efficient nucleic acid detection in combination with LAMP in a single reaction workflow, setting the basis for development of point-of-care tests.

Graphical abstract



Introduction

The Cas12 enzymes are programmable single effector nucleases of the CRISPR–Cas type V family that rely on guide RNA spacers (~20 nt) to recognize complementary target DNA [1, 2]. A distinctive feature of Cas12 nucleases is their dual nuclease activity: upon specific recognition of a target DNA by a complementary guide RNA (crRNA, *cis* activity), the enzyme is activated to indiscriminately cleave nearby nucleic acids (*trans* activity) (Fig. 1A) [3, 4]. The combination of precise target recognition and collateral cleavage has been leveraged in nucleic acid diagnostics, where *cis* activity confers high specificity, and *trans* activity enables simple and sensitive signal readout [5–8]. For instance, in fluorescence-based tests, the presence of a target is detected through the cleavage of

fluorescently labeled reporters by *trans* activity, resulting in a measurable fluorescent signal (Fig. 1A). While Cas12a-based nucleic acid detection offers high specificity through guide-directed recognition, its intrinsic sensitivity restricts its application to high-abundance target differentiation, such as genotyping, and is often insufficient for direct detection of low-abundance targets. To overcome this limitation, many Cas12-based molecular diagnostics have been coupled with isothermal nucleic acid amplification methods to preamplify target prior to detection.

Loop-mediated isothermal amplification (LAMP) is a powerful amplification method that uses a strand-displacing DNA polymerase and 4–6 primers to rapidly produce large amounts of DNA at a constant temperature (around 65°C) [9, 10]. It

Received: March 6, 2025. Revised: May 20, 2025. Editorial Decision: May 22, 2025. Accepted: May 29, 2025

© The Author(s) 2025. Published by Oxford University Press on behalf of Nucleic Acids Research.

This is an Open Access article distributed under the terms of the Creative Commons Attribution-NonCommercial License

(https://creativecommons.org/licenses/by-nc/4.0/), which permits non-commercial re-use, distribution, and reproduction in any medium, provided the original work is properly cited. For commercial re-use, please contact reprints@oup.com for reprints and translation rights for reprints. All other permissions can be obtained through our RightsLink service via the Permissions link on the article page on our site—for further information please contact journals.permissions@oup.com.

is widely used for sensitive and specific molecular diagnostics due to its rapid turnaround time, low cost, tolerance to inhibitors, and flexible readout methods [11–14]. When combined with Cas12a, its detection specificity can be further improved [5, 15, 16]. However, differences in optimal reaction conditions between these two systems often require that LAMP and Cas reactions take place in two separate reactions (two-pot), increasing hands-on time and the risk of carryover contamination. Thus, assays that couple the two reactions in a single reaction mixture (one-pot) are preferred to minimize sample handling and streamline the process.

Molecular diagnostics combining LAMP with thermostable Cas12b in one-pot format have been reported [6, 7], but Cas12b guide RNAs are long (>110 nt), increasing cost, time, and complexity to the tests. In contrast, Cas12a uses much shorter guide RNAs (~40 nt), which are easier and cheaper to synthesize. While LAMP–Cas12a tandem (two-pot) assays have been effective [5, 17–19], one-pot reactions has been less efficient due to the requirement of suboptimal LAMP temperatures [20]. Further, additional steps, such as addition of pyrophosphatase and primer phosphorothioate modification, are required to compensate for Cas12a's lack of thermostability [20]. Therefore, a thermostable, highly active Cas12a is ideal for robust one-pot Cas12a–LAMP-coupled molecular diagnostics.

Recently, a large-scale protein language-model based prediction method has been deployed to survey the natural Class II Cas effectors [21]. It is predicted that Cas12a nucleases are not stable at temperatures >60°C, with only a small subset stable between 55°C and 60°C. To overcome this, we focused on the thermostable Cas12a ortholog YmeCas12a (from *Yellowstone metagenome*) to develop strategies for one-pot LAMP–Cas12a enabled nucleic acid diagnostics [22]. Through kinetic comparison with the highly active mesophilic LbaCas12a (from *Lachnospiraceae bacterium ND 2006*) [23, 24], we determined that YmeCas12a *trans* nuclease activity is limited by its poor affinity to the *trans* substrate. Thus, we engineered YmeCas12a by structure-guided mutagenesis and introduced positively charged residues in the Nuc and RuvC domains to facilitate *trans* substrate binding. The Cas12a *trans* nuclease activity was also improved by fusion to DNA-binding proteins (DBPs). Combinatorial variants of these strategies further improved the *trans* nuclease activity, enabling us to realize efficient one-pot detection of target RNA to as low as 5 copies/μl. The strategies described here can be extended to other Cas12a nucleases and deployed for applications that require high *trans* nuclease activity as well.

Materials and methods

Reagents and common procedures

EnGen® Lba Cas12a (#M0653T), Monarch® PCR & DNA Cleanup Kit (#T1130), Q5® Hot Start High-Fidelity 2× Master Mix (#M0494L), NEBuilder HiFi DNA Assembly Cloning Kit (#E5520), DNase I (#m0303S), Micrococcal Nuclease (#m0247S), NEBuffer™ r2.1 (#B6002S), Proteinase K (#P8107S), Bst 2.0® DNA polymerase (#M0537S), Isothermal Amplification Buffer (#B0537S), WarmStart® RTx Reverse Transcriptase (#M0380L), dNTP solution mix (#N0447L), Lambda DNA (#N3011S), and Recombinant Albumin, Molecular Biology Grade (#B9200S) were all from New England Biolabs (Ipswich, MA, USA). SYTO™ 82 (#S11363)

was from ThermoFisher. Synthetic SARS-CoV-2 RNA (Control 2, #102024) was purchased from Twist Bioscience (CA, USA). Jurkat cell total RNA (#R1255815-50) was from Biochain (CA, USA).

YmeCas12a and its variants used in this study were purified using standard liquid chromatography protein purification techniques following the published procedures until at least 90% purity by acrylamide gel [22], with minor modifications when necessary. Purified proteins were stored at –20 °C in a buffer consisting of 20 mM Tris–HCl at pH 7.5 (25°C), 500 mM NaCl, 1 mM DTT, and 50% glycerol (v/v) until use.

All concentrations shown are final concentrations in the reaction. All Cas12a nuclease assays were carried out either in 1× NEBuffer r2.1 (10 mM Tris–HCl, pH 7.9 at 25°C, 50 mM NaCl, 10 mM Mg²⁺, and 100 μg/ml recombinant Albumin) or a buffer formulated the same except for the exclusion of NaCl. The Cas12a–crRNA (RNP) complex was prepared by mixing Cas12a and crRNA at 1:1.5 molar ratio in 1× NEBuffer r2.1 supplemented with 1 mM tris(2-carboxyethyl)phosphine (TCEP) and pre-incubated at room temperature for 15 min before inclusion in the subsequent steps. Cas12a nuclease *cis* cleavage results were resolved by capillary electrophoresis on an Agilent 2100 Bioanalyzer (Agilent Technologies, Santa Clara, CA), and the results were analyzed with Peak Scanner™ software (Applied Biosystems, Foster City, CA).

DNA and crRNA preparation

All DNA oligonucleotides, fluorescent reporters, and crRNAs were obtained from Integrated DNA Technologies (Coralville, IA) and sequences are listed in [Supplementary Table S1](#). The *cis* substrate for Cas12a was double strand (dsDNA) product (E1-PCR) purified from PCR reactions; the *trans* substrate was NZ-GT reporter unless specified otherwise. The guide RNAs (crRNAs) were designed by appending a 20-nt spacer sequence to the natural scaffold sequences of LbaCas12a or YmeCas12a according to previous publications [22, 24]. The lyophilized synthetic crRNAs were resuspended in RNA annealing buffer (10 mM Tris–HCl, pH 7.5, 50 mM NaCl, and 1 mM EDTA) and refolded by heating to 80°C for 2 min followed by slow cooling at a rate of 0.1 °C/s until 25°C. Aliquots were stored at –20°C until use.

Thermostability test of Cas12a proteins

The thermostability of Cas12a proteins was measured by the denaturing temperature on a Prometheus nano differential scanning fluorimetry (nanoDSF, Monotemper, Munich, Germany) instrument following published procedure [22]. The inflection point is interpreted as the unfolding/melting point of the apo protein or ribonucleoprotein (RNP).

Alternatively, the thermostability of RNP was determined by the *trans* cleavage rate after heat challenge. Specifically, 30 nM pre-formed RNP (with crRNA4) was aliquoted and incubated at 55.1°C, 58.4°C, 60.9°C, or 64°C in a thermocycler for 5, 10, or 20 min before removal to ice. One aliquot without heat treatment was used as a control. After all treatments were complete and incubated on ice for at least 5 min, pre-cooled *cis* substrate (1 nM) and *trans* substrate (200 nM) were added to the reactions. The reactions were aliquoted to 3× repeats on a 96-well plate and incubated at the corresponding challenge temperatures (to mimic a one-pot reaction scenario) on a Bio-Rad CFX 96 real-time instruments (Bio-Rad, Hercules CA, USA). Fluorescence was scanned on the SYBR channel

every 30 s. Each plate reading cycle was considered 7 s. The *trans* cleavage rates were obtained by linear fit of the fluorescence change over time at the initial reaction time (before 20 cycles) when fluorescence increase was in the linear range.

Nucleic acid detection reactions by standalone RT-LAMP or RT-LAMP coupled with Cas12a

All reactions were set up on ice until incubation on a Bio-Rad CFX 96 real-time instrument. Reverse transcription-LAMP (RT-LAMP) reactions were set up following standard protocols with minor changes. Specifically, each 50 μ l of reaction comprises 1 \times Isothermal Amplification buffer, 8 mM MgSO₄ (10 mM total Mg²⁺), 1.4 mM of each dNTP, 1 \times LAMP primer mix (0.2 μ M F3, 0.2 μ M B3, 1.6 μ M FIP, 1.6 μ M BIP, 0.4 μ M Loop F, 0.4 μ M Loop B), 16 U Bst[®] 2.0 DNA polymerase, 15 U WarmStart[®] RTx Reverse Transcriptase, 1 μ M of SYTO[™] 82, with the addition of 2 μ l of RNA as target or Jurkat RNA as control. The reactions were aliquoted to 3 \times wells (15 μ l each) in a 96-well plate and incubated on a Bio-Rad CFX 96 real-time instrument. Fluorescence was recorded in all channels every 30 s. The RT-LAMP reaction was monitored by fluorescence from SYTO[™] 82 intercalating dye binding to the dsDNA product in the HEX channel. Each plate reading was considered to take 11 s.

The RT-LAMP and Cas12a coupled one-pot reactions were the same as RT-LAMP reactions except that each 50 μ l of reaction also included 1 μ M NZ-GT reporter and 100 nM Cas12a RNP. The Cas12a reaction was monitored by fluorescein (FAM) fluorescence from release of the FAM fluorophore upon Cas12a nuclease cleavage of the NZ-GT reporter in the FAM channel, and the RT-LAMP reaction was monitored in the HEX channel simultaneously. Assays coupling LAMP and Cas12a targeting DNA target were carried out with the same procedure and condition except for the omission of reverse transcriptase in the reactions.

The RT-LAMP and Cas12a coupled two-pot reactions were set up in two steps. After RT-LAMP reaction incubated at 58 $^{\circ}$ C, 1 μ l of the product was added to a Cas12a reaction pre-incubated on ice to make a final volume of 50 μ l. The Cas12a reaction was comprised of 1 \times NEBuffer r2.1, 500 nM NZ-GT reporter, 50 nM RNP (YmeCas12a complexed with cr-RNA4), and supplemented with either 1 \times LAMP primer mix, 16 U Bst[®] 2.0 DNA polymerase, 1.4 mM of each dNTP, or water. Each reaction was aliquoted 15 μ l each to three wells in a 96-well plate and incubated at 55 $^{\circ}$ C on Bio-Rad CFX 96. Fluorescence was recorded in the SYBR channel every 30 s. Each plate reading cycle was considered to take 7 s.

Cas12a *trans* cleavage kinetic assay

Cas12a *trans* cleavage reaction was designed in pseudo-first order reaction condition with excess reporter and limiting RNP–DNA *cis* complex, the latter of which was established by using limiting amount of *cis* dsDNA with excess RNP. The same amount of limiting *cis* dsDNA was used for direct comparison of *trans* cleavage efficiency of different enzymes. Specifically, the RNP (50 nM) was formed in 1 \times NEBuffer r2.1 (without NaCl) in the presence of 1 mM TCEP and supplemented with NaCl to a final concentration of 50 mM after inclusion of the NaCl carryover from the enzyme storage buffer. Modulation of *trans* nuclease activity by dNTPs or NaCl was tested by inclusion of dNTPs or NaCl at the concentration specified in the corresponding figures. After 15-

min incubation at the room temperature, the RNP was put on ice and added with 200 nM reporter and 2 or 5 nM *cis* DNA (specified in figure legend). The reaction mixture was aliquoted to at least 3 \times wells on a 96-well plate to incubate on a Bio-Rad CFX 96 following a general protocol: initial incubation at 55 $^{\circ}$ C for 10 s followed by 100 cycles of 55 $^{\circ}$ C for 30 s (unless specified otherwise) plus plate read by the SYBR channel.

The *trans* nuclease reaction rates were obtained from initial data points when fluorescence signal increase was in the linear range, by fitting a linear regression formula:

$$y = kx + a$$

Where a is the fluorescence at the earliest time point, and k is the slope (Δ RFU/cycle) representing the initial rate for *trans* nuclease activity when reaction was in the steady state.

Cas12a *cis*-cleavage kinetic assay

To determine the *cis* nuclease kinetics, Cas12a reactions were carried out under single-turnover condition with excess active RNP and limiting DNA. All assays were carried out with perfectly-matched *cis* dsDNA substrate E1-PCR, which has a 5'-HEX on the target strand and 5'-FAM on the nontarget strand to monitor cleavage of both strands.

The active site titration experiments were carried out as described before for Cas9 nucleases with minor modifications [25, 26]. Due to the *trans* nuclease activity on dsDNA, the *cis* substrate could be digested by activated Cas12a so care was taken to limit reactions to a short time, or reactions were performed with 150 mM NaCl to reduce *trans* activity.

The *cis* cleavage rate of Cas12a was determined by rapidly mixing a pre-formed RNP complex (60 nM, active RNP) with an equal volume of DNA (20 nM) in 1 \times NEBuffer r2.1 using a KinTek RQF-3 (KinTek Corporation, Snow Shoe, PA) at either 55 $^{\circ}$ C (YmeCas12a and variants of) or 37 $^{\circ}$ C (LbaCas12a). The reaction was allowed to proceed for the specified period before quenching with 100 mM EDTA, then supplied with 0.1 unit of Proteinase K at 37 $^{\circ}$ C for 15 min to release DNA. Reactions were diluted 5 \times with water for cleavage analysis by capillary electrophoresis [27].

The catalysis rate was obtained by fitting the time dependence of product formation with a single exponential equation:

$$[DNA]_{\text{cleaved}} = A \times (1 - e^{-kt})$$

Where A is the amplitude, and k is the observed cleavage rate on *cis* dsDNA substrate $k_{\text{obs,cis}}$. Since the *cis* cleavage kinetics are carried out by mixing RNP with dsDNA in the presence of divalent cation Mg²⁺, the reaction undergoes processes including, but not limited to, R-loop formation, enzyme conformational changes, as well as scission of the phosphodiester bonds. Thus, $k_{\text{obs,cis}}$ represents a lower limit of actual catalytic rate of the RuvC nuclease, and we use this rate to reflect the activation rate of RuvC nuclease by the *cis* substrate (as compared to activation by *trans* substrate in the *trans* cleavage kinetic assay). All *cis* kinetic parameters are listed in [Supplementary Table S2](#).

Michaelis–Menten kinetics

After formation at room temperature, the RNP was cooled on ice. Subsequent reaction setup was carried out on ice. The RNP–DNA *cis* complex was prepared by mixing 20 nM pre-

formed RNP with 1 nM *cis* substrate, then mixed with the reporter varying between 50 nM and 8000 nM, as indicated in figure legends. Each reaction was aliquoted to 5× wells in a 96-well plate and incubated on a Bio-Rad CFX 96 instrument preheated at 37°C (for LbaCas12a) or 55°C (for YmeCas12a and its variants). Fluorescence signal was obtained every 30 s in the SYBR channel. Background-subtracted fluorescence was obtained by subtracting the buffer-only sample from the raw fluorescence readings from each reaction. Average of the background-subtracted fluorescence from all five repeats was then converted to reporter concentration calibrated from a standard curve and plotted against time. The initial data points were fitted with a linear regression to obtain initial reaction velocity (nM/s). The initial velocities were further plotted against the reporter concentration and fitted with Michaelis–Menten equation:

$$v/[E]_0 = (k_{\text{cat}} \times [S]) / (K_m + [S])$$

Where v is the initial reaction velocity, E_0 is the total enzyme concentration (RNP–DNA *cis* complex, 1 nM, determined by the limiting *cis* DNA concentration in the bimolecular reaction), S is the *trans* substrate (reporter) concentration. From this equation, we obtain the steady-state kinetic parameters K_m and k_{cat} . The Michaelis constant K_m is not a direct measurement of substrate binding affinity, but a reasonable approximation without detailed information on the *trans* cleavage mechanism. The parameter k_{cat} represents the apparent catalytic rate of *trans* nuclease activity on the *trans* substrate, which is a lower limit on the true catalytic rate of the *trans* substrate. The specificity constant, k_{cat}/K_m , is obtained by division of the two. Note that in this study, K_m and k_{cat} obtained from Michaelis–Menten plot refer to the *trans* nuclease activity specifically and not the *cis* activity.

The standard curve was generated by digesting the reporter series of 50, 120, 200, 300, 400, 500, 600, and 700 nM with 2 unit of Dnase I at 37°C for 30 min. After the 30-min incubation, the reactions were moved to a Bio-Rad CFX 96 and monitored fluorescence in SYBR channel for 15 cycles. Fluorescence signals from cycles 4–11 were averaged to minimize random drift of signal and subtracted of the background fluorescence from buffer-only samples. The reaction plate was kept at room temperature in dark after the initial plate reading and monitored the fluorescence again after 3 h. There was no change in the fluorescence readout, indicating that the digestion was complete. All Michaelis–Menten kinetic parameters are listed in [Supplementary Table S3](#).

Structural analysis of YmeCas12a

AlphaFold2 structure predictions of YmeCas12a were performed using the Colabfold platform [28, 29]. Plots for multiple sequence alignment coverage and predicted Local Distance Difference Test (pLDDT) for each residue can be found in [Supplementary Fig. S9](#). Rank_1 was selected from the top 5 ranked predictions for subsequent analysis due to its low predicted aligned error (PAE) score and conformational similarity to the experimentally established post-*cis* Cas12a structures that we are interested in this study. The confident and continuous pLDDT scores across each domain of the YmeCas12a predicted structure ([Supplementary Fig. S9](#)) was sufficient to facilitate hypothesis generation for rational engineering. The predicted structure was compared to X-ray crystal structures of Cas12a in complex with guide RNA and *cis* DNA, specif-

ically the *Lachnospiraceae bacterium* Cas12a (LbaCas12a) complex with crRNA and tsDNA (PDB: 5XUS) and the *Francisella novicida* Cas12a (FnoCas12a) complex with crRNA guide and dsDNA target substrate (PDB: 6I1K) [30, 31]. Structural superimpositions of the YmeCas12a predicted structure to the experimental structures were performed for C α atoms with the align algorithm in PyMol (The PyMOL Molecular Graphics System, version 2.0 Schrödinger, LLC) with default parameters. PyMOL was used for structural interpretation and illustration.

Mutagenesis

Mutagenesis of YmeCas12a was carried out with the expression plasmid for YmeCas12a by using a Q5[®] site directed mutagenesis kit or NEBuilder[®] HiFi assembly following the recommended procedures. Oligo nucleotides used for mutagenesis are listed in [Supplementary Table S1](#).

Results and discussion

Wild-type YmeCas12a cannot enable efficient LAMP-coupled one-pot nucleic acid detection

The LAMP reaction requires incubation at a single temperature near 65°C. To assess the feasibility of one-pot LAMP–Cas12a coupled test, we decided to pair LAMP with a previously reported thermostable Cas12a ortholog YmeCas12a [22], which denatures at ~66°C as Cas12a–crRNA RNP. Considering that the RNP needs to be activated by the LAMP product (*cis* substrate) before cleaving the fluorescent reporter (*trans* substrate, Fig. 1A) in a one-pot workflow, we first investigated the durability of the RNP activity at high temperatures. The *trans* nuclease activity was monitored after incubating the RNP between 55°C and 64°C for 5, 10, and 20 min or with no heat treatment (0 min, as control) before addition of the *cis* (target DNA) and *trans* (intramolecularly quenched FAM-containing reporter) substrates, which generates FAM signal upon cleavage ([Supplementary Fig. S1a](#)). We observed that the YmeCas12a RNP complex maintained high activity for up to 20 min at 55–58°C and gradually lost activity at higher temperatures, consistent with previous results ([Supplementary Fig. S1a](#), left) [22]. In contrast, the RNP of mesophilic ortholog LbaCas12a was almost completely inactive after 5-min incubation at 55°C ([Supplementary Fig. S1b](#), right). The overlap in working temperatures of YmeCas12a and LAMP reactions provided an opportunity to establish LAMP–Cas one-pot nucleic acid detection. Indeed, in a one-pot reaction that couples RT-LAMP and YmeCas12a, FAM fluorescence from YmeCas12a *trans* cleavage of the reporter was observed when target RNA was present (Fig. 1B and [Supplementary Fig. S2](#)). The onset of Cas12a signal coincided with the SYTO 82 signal that monitored dsDNA formation from the LAMP reaction, indicating that significant accumulation of the LAMP product was needed to activate Cas12a for *trans* cleavage activity.

Interestingly, when a small amount (1 μ l) of the LAMP reaction product was added to a Cas12a reaction (50 μ l) in a two-pot assay, robust FAM signal from Cas12a reaction was observed immediately, in contrast to the weaker signal from the one-pot assay (compare Fig. 1B and C). This implies that LAMP reaction components inhibit Cas12a activity in the one-pot context. To test this hypothesis, we individually added each of the main LAMP reaction components

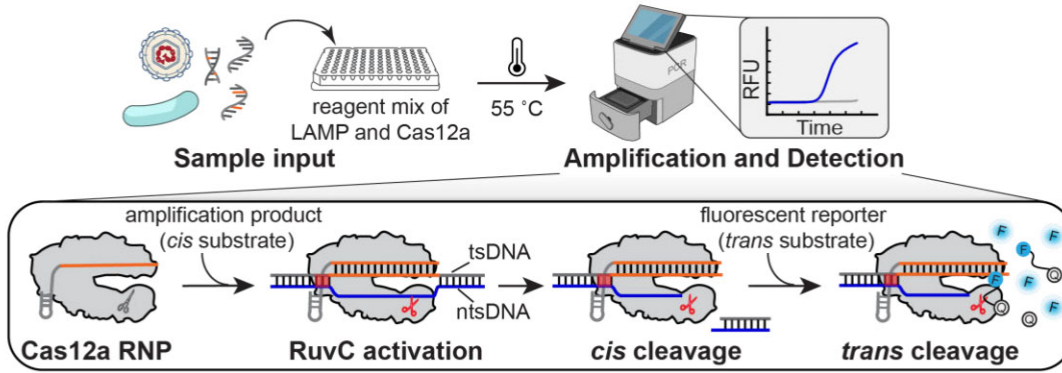
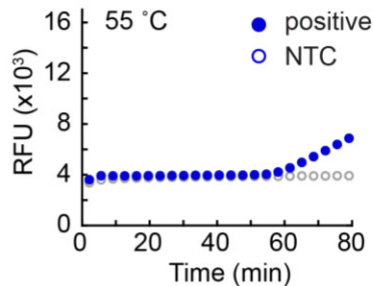
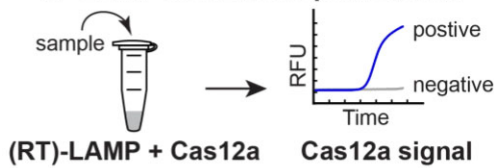
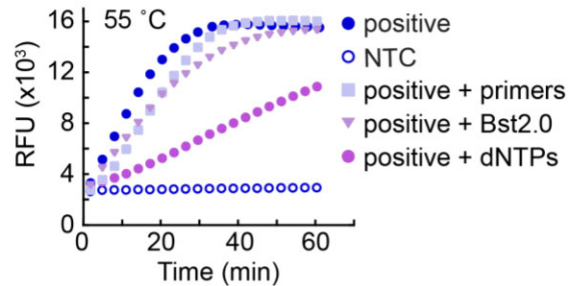
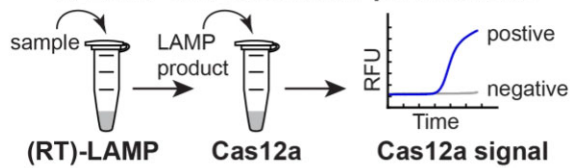
A LAMP-Cas12a one-pot nucleic acid detection**B LAMP-Cas12a one-pot reaction****C LAMP and Cas12a two-pot reactions**

Figure 1. Performance of YmeCas12a wild-type in LAMP–Cas12a coupled reactions. **(A)** Schematic of nucleic acid detection by LAMP–Cas12a coupled one-pot reaction. After sample addition, the reaction mixture containing both LAMP and Cas12a reagents was incubated at a constant temperature for amplification (LAMP reaction) and detection (Cas12a reaction) in a single reaction workflow. Cas12a-mediated detection was enabled by crRNA-guided specific recognition of the *cis* substrate (LAMP product) and subsequent nonspecific *trans* cleavage of a fluorescent reporter. The reporter fluorescent signal indicates the presence of the target nucleic acid in the sample. **(B)** Performance of YmeCas12a wild-type in the RT-LAMP–Cas12a one-pot reaction in detection of RNA. Traces shown are FAM fluorescence generated from Cas12a *trans* cleavage of the reporter. In one-pot reactions, components for both RT-LAMP and YmeCas12a were prepared in a single reaction mixture. After addition of the substrate, reactions were incubated at 55 °C to monitor the FAM fluorescence. Synthetic RNA substrate diluted in 5 ng/μl Jurkat RNA was used as positive control at 200 copies/μl. Jurkat RNA was used as no-template control (NTC). **(C)** Performance of YmeCas12a in the two-pot reactions with RT-LAMP followed by Cas12a in detection of target RNA. RT-LAMP reaction was set up the same way as for one-pot, except for the omission of Cas12a components. After RT-LAMP reaction, 1 μl of product was removed to a 50 μl of Cas12a reaction to monitor the FAM fluorescence from the reporter. The Cas12a reaction was added with either LAMP product only (positive or NTC), or positive product supplemented with the indicated component in the same concentration as in one-pot reactions.

to the Cas12a reaction in a two-pot assay. We observed that the inclusion of dNTPs significantly inhibited Cas12a signal (Fig. 1C), consistent with a previous report [17]. Conversely, Cas12a appeared to inhibit the LAMP reaction in the one-pot setup, as evidenced by the delayed LAMP signal onset in the one-pot reaction compared to the LAMP-only reactions (Supplementary Fig. S2). These results reflect the competition between the two reactions. In one-pot reactions, Cas12a binds and cleaves the LAMP product, inhibiting amplification, while high dNTP concentrations support LAMP but inhibit Cas12a activity. Additionally, Bst DNA polymerase may displace Cas12a from the *cis* product, further disrupting Cas12a activity, as seen in studies of Cas9 and DNA polymerase interactions [32]. Therefore, careful balancing of the two reactions is required for successful one-pot assay. While YmeCas12a showed sufficient thermostability and *trans* nu-

lease activity for detectable signals, the one-pot reaction requires further optimization for efficient molecular diagnostic purpose.

YmeCas12a shows less efficient *trans* nuclease activity than LbaCas12a

To optimize the one-pot reaction, we decided to analyze the *trans* nuclease kinetics of YmeCas12a and compare it to the well-studied mesophilic and highly active LbaCas12a. Four target sites were designed on the SARS-CoV-2 E gene of the previously reported LAMP amplicon with a TTTV protospacer adjacent motif (PAM) (Fig. 2A) [33], which is compatible with both Cas12a enzymes (YmeCas12a requires a TTV PAM and LbaCas12a requires a TTTV PAM) [22, 30]. We then compared the *trans* nuclease activities of YmeCas12a and

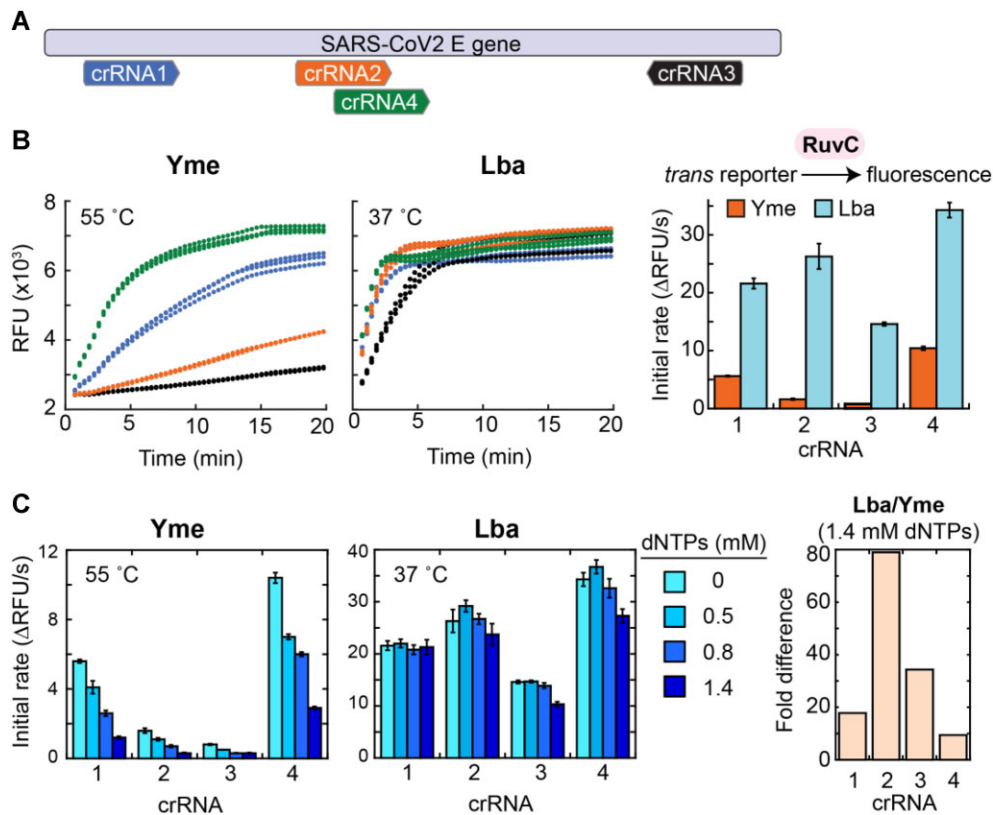


Figure 2. YmeCas12a is less efficient than LbaCas12a in cleavage of the *trans* substrate. **(A)** Schematic of SARS-CoV-2 E gene LAMP amplicon with four guide RNAs designed to be compatible with both YmeCas12a and LbaCas12a for comparative studies. **(B)** Example traces showing the *trans* nuclease activity of YmeCas12a and LbaCas12a at the four target sites. Cas12a (50 nM) was complexed with each of the four different crRNAs (100 nM, same color code as in panel (A)), activated by 5 nM *cis* dsDNA, and incubated with excess reporter (200 nM) to monitor the *trans* cleavage activity. The *trans* cleavage rates calculated from the initial time when fluorescence change was linear are shown on the right. **(C)** Effect of dNTPs on the initial *trans* cleavage rates. Reactions were performed under the same condition as for panel (B) except for the inclusion of dNTPs. Note that a typical LAMP reaction includes 1.4 mM each dNTP. Fold difference in the initial *trans* cleavage rates of YmeCas12a in comparison to LbaCas12a in the presence of 1.4 mM dNTPs is shown on the right. Error bars represent standard deviation from two independent experiments.

LbaCas12a at their respective optimal reaction temperatures (Fig. 2B). Cas12a was loaded with each guide to form RNP (50 nM), activated by a limiting amount of *cis* DNA (2 nM), and then allowed to react with excess *trans* reporter (200 nM). Thus, the initial rate of the relative fluorescence unit change (Δ RFU) approximates the *trans* nuclease activity of the specific RNP independent of the RNP concentration. The *trans* nuclease activity of YmeCas12a showed marked differences among the four guides (13-fold, 0.8–10.4 Δ RFU/min, Fig. 2B). Comparatively, LbaCas12a showed 2–20 times higher activity with less variation among the guides (2-fold, 14.6–34.3 Δ RFU/min). It is worth noting that crRNA4, the guide with the highest *trans* nuclease activity, was the only guide that enabled YmeCas12a in LAMP–Cas one-pot detection of SARS-CoV-2 (Supplementary Fig. S3a), implying that high Cas12a *trans* nuclease activity is a prerequisite for successful one-pot nucleic acid detection.

We further tested the *trans* nuclease activities of YmeCas12a and LbaCas12a in the presence of dNTPs. The *trans* nuclease activity of YmeCas12a showed inhibition by dNTPs in a dose-dependent manner, whereas LbaCas12a seemed more tolerant to the dNTPs (Fig. 2C). Specifically, in the presence of 1.4 mM dNTPs, the typical concentration in a LAMP reaction, YmeCas12a showed ~10- to 80-fold lower activity than LbaCas12a. We titrated dNTPs in the

one-pot reaction and found that, despite the inhibition, Cas12a exhibited higher signal in the presence of higher dNTP concentration (Supplementary Fig. S3b, left). This was likely due to the more efficient LAMP reactions (faster LAMP signal) driven by higher dNTPs (Supplementary Fig. S3b, right). Therefore, inhibition of YmeCas12a *trans* activity by dNTPs, the essential component for LAMP reaction, may pose a challenge for one-pot integration. A similar inhibitory trend of the *trans* activity was also observed by monovalent salt NaCl (Supplementary Fig. S4), which suggests that binding of the *trans* substrate could be limiting YmeCas12a activity under these conditions. Considering that high dNTPs is required for efficient LAMP reactions, we decided to characterize YmeCas12a in greater detail instead of focusing on optimizing the one-pot reaction condition. We reasoned that a better understanding on the mechanisms governing *trans* nuclease activity in general would be useful for developing strategies to improve the activity.

The RuvC nuclease of YmeCas12a is not intrinsically less efficient than that of LbaCas12a by *cis* reaction kinetics

The distinct *trans* nuclease activities of YmeCas12a and LbaCas12a in response to increasing concentrations of dNTPs

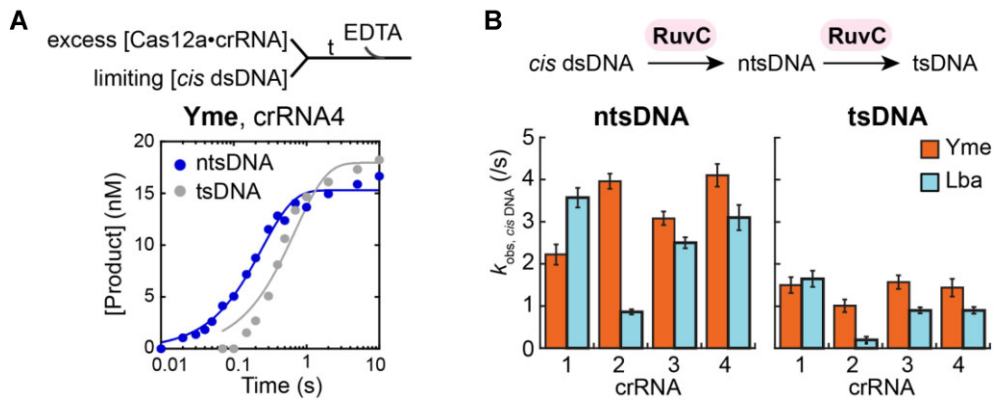


Figure 3. YmeCas12a initiates *cis* cleavage as efficiently as LbaCas12a. **(A)** Example time course of *cis* dsDNA cleavage by YmeCas12a. Single turnover reactions were carried out with excess active RNP (60 nM) and limiting *cis* dsDNA (20 nM) in the presence of 10 mM Mg²⁺. Reactions were quenched with 100 mM EDTA at different time points. Reaction products of both strands of the *cis* dsDNA were measured (dots) and fit with a single exponential equation (lines). **(B)** Comparison of the observed *cis* cleavage rates of YmeCas12a and LbaCas12a. The RuvC nuclease domain sequentially cleaves the ntsDNA and tsDNA before *trans* activity; so, kinetics of both strands were compared. Error bars represent standard deviation from numeric fitting of results from a single experiment. Full dataset can be found in [Supplementary Table S2](#).

and NaCl and across different targets indicated that the regulation of the two effectors is different. Since the single RuvC nuclease domain is responsible for sequential *cis* and *trans* nuclease activities (Fig. 1A) [3, 31, 34, 35], we hypothesized that the observed *trans* nuclease differences reflect the intrinsic differences in the respective RuvC nucleases. If true, we should expect the two enzymes to show distinct *cis* activities correlated to the *trans* activities. Therefore, we determined the reaction kinetics of the *cis* substrate cleavage for the two enzymes. Specifically, single-turnover reactions with excess RNP (60 nM active RNP) and limiting *cis* dsDNA substrate (20 nM) were performed in a rapid quench instrument. Reactions were carried out for 0.01–10 s before quenching. The rates of *cis* cleavage reaction were obtained by plotting the amount of product generated over time and fitting with a single exponential equation (Fig. 3A; [Supplementary Fig. S5](#) and [Supplementary Table S2](#)).

The RuvC nuclease cleaves *cis* dsDNA sequentially (Fig. 3B, top) [35–39]. The nontarget strand DNA (ntsDNA) is positioned at the active site after R-loop formation, ready for cleavage (Fig. 1A). Following ntsDNA cleavage, conformational changes reposition the target strand DNA (tsDNA) in the active site. Thus, the intrinsic RuvC nuclease kinetics are likely reflected by the cleavage kinetics of the ntsDNA (and not the tsDNA). Regardless, we plotted the cleavage rates of both DNA strands when YmeCas12a and LbaCas12a were loaded with the different guides (Fig. 3B, bottom). Comparison of the ntsDNA cleavage rates showed that YmeCas12a initiated *cis* target cleavage faster than LbaCas12a in three out of the four tested guides. Similarly, YmeCas12a-mediated cleavage of the tsDNA was at least as fast as that of LbaCas12a. These results indicated that the *cis* DNA substrate activates YmeCas12a at least as efficiently as LbaCas12a. This is in stark contrast to, instead of in correlation with, the observed *trans* cleavage kinetics (compare Figs. 3B and 2B). The lack of correlation between the *cis* and *trans* cleavage rates further imply that these two activities are relatively uncoupled, despite both being catalyzed by the same RuvC nuclease. Therefore, to gain deeper insight into the factors that specifically limit *trans* nuclease activity, we focused on the YmeCas12a post-*cis* cleavage reaction kinetics.

YmeCas12a *trans* nuclease activity is limited by its affinity to the *trans* substrate

Since Cas12a *trans* nuclease activity appeared to be relatively uncoupled from its *cis* activity, we decided to isolate the enzyme in its *trans* nuclease state to better characterize the *trans* cleavage kinetics. Without the *trans* substrate, the post-*cis* complex was found to be stable for >4 h at room temperature in a *trans*-active state ([Supplementary Fig. S6](#)). We examined the steady-state kinetics of the *trans* nuclease activity for both LbaCas12a and YmeCas12a by mixing a limiting amount of post-*cis* complex (1 nM) with excess *trans* reporter in varying concentrations (50–4000 nM) (Fig. 4A, and [Supplementary Fig. S7](#)). Comparing the same target (crRNA2), YmeCas12a showed a ~4-fold lower catalytic efficiency (k_{cat}) relative to LbaCas12a, and its approximate affinity to the *trans* substrate (K_m) was 20-fold lower. The differences in catalysis and affinity lead to 77 times lower specific activity (k_{cat}/K_m) of YmeCas12a compared to LbaCas12a (Fig. 4B), in agreement with the earlier observations (Fig. 2B). Since YmeCas12a showed variable *trans* cleavage activities across targets (Fig. 2B), we further investigated the steady-state kinetics of YmeCas12a with the other three guides (Fig. 4C; [Supplementary Fig. S7](#) and [Supplementary Table S3](#)). Among the four guides, the kinetic parameters for catalytic efficiency (k_{cat}) and the affinity to the *trans* substrate (K_m) was ~4- and 11-fold difference, respectively, which led to ~48-fold difference in specific activity (k_{cat}/K_m). Together, these results suggest that *trans* substrate affinity is the main determinant for *trans* nuclease activity of YmeCas12a, and it explains the differences in *trans* activity variations between guides and its lower *trans* activity compared to LbaCas12a.

To ensure the observed activity of YmeCas12a was not biased by the structured reporter (NZ-GT) in these tests, which was selected for high *trans* activity with LbaCas12a with low background [40], we also performed steady state kinetic analyses using the linear reporter T25 ([Supplementary Fig. S8](#) and [Supplementary Table S3](#)). Consistent with the NZ-GT reporter, the activity of YmeCas12a with the T25 reporter showed guide-dependent variations in specific activity (k_{cat}/K_m , 16-fold), mainly driven by the differences in K_m (8-fold) rather than k_{cat} (2-fold). These results indicate that poor

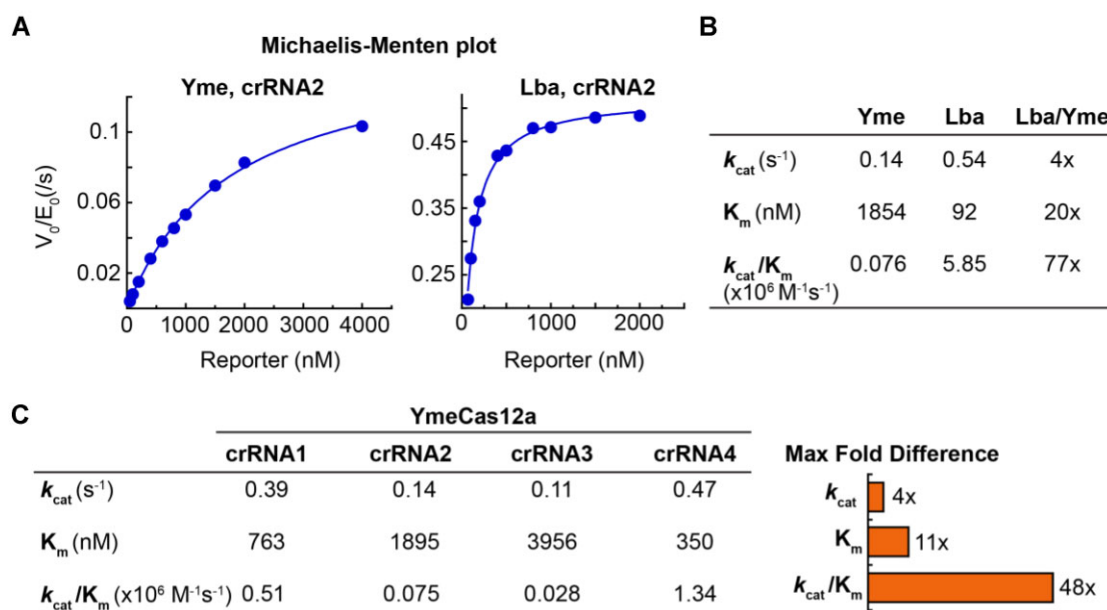


Figure 4. YmeCas12a *trans* cleavage kinetics is restricted by poor binding (K_m) to the *trans* substrate. **(A)** Michaelis–Menten kinetics of YmeCas12a and LbaCas12a on the *trans* substrate at the same *cis* target site (both with crRNA2). Data point was shown as dot, and the curve fitting was shown as line. **(B)** Fold difference of the Michaelis–Menten kinetic parameters between YmeCas12a and LbaCas12a. **(C)** Comparison of Michaelis–Menten kinetic parameters of YmeCas12a at four different target sites. Maximum fold difference between the four sites is shown on the right. All steady-state kinetic reactions on the *trans* substrate were carried out with limiting RNP–DNA complex (E_0 , 1 nM) with excess *trans* substrate ranging from 50 to 4000 nM to obtain the initial *trans* cleavage rates (V_0 , nM/s). The initial velocities were further plotted against the reporter concentration and fitted with Michaelis–Menten equation to obtain the Michaelis–Menten kinetic parameters k_{cat} and K_m . Parameters k_{cat} and K_m were averaged from at least two independent repeats. Errors from fitting were not shown for simplicity. Full dataset can be found in [Supplementary Table S3](#).

trans substrate binding appears to be the primary constraint on YmeCas12a *trans* activity. Therefore, we focused on improving the *trans* nuclease activity by enhancing *trans* substrate binding.

Engineering the helix-loop-helix motif improves YmeCas12a *trans* nuclease activity

A structural model of YmeCas12a was generated with AlphaFold2 (Fig. 5A and [Supplementary Fig. S9](#)), and compared with X-ray crystal structures of two orthologs in post-*cis* cleavage states. The predicted YmeCas12a structure aligned well with that of LbaCas12a in complex with crRNA and tsDNA (PDB: 5XUS; $RMSD_{C\alpha} = 3.0 \text{ \AA}$) and FnoCas12a in complex with crRNA and both strands of *cis* dsDNA (PDB: 6I1K; $RMSD_{C\alpha} = 4.9 \text{ \AA}$) [30, 31].

Structural analysis highlighted variation in the helix-loop-helix (HLH) region of the REC1 domain (Fig. 5B, top), which rotates after *cis* substrate binding and directs substrate DNA to the nuclease (Nuc) lobe [36, 38]. The YmeCas12a HLH motif was extended relative to LbaCas12a and FnoCas12a (Fig. 5B, middle). Of note, the longer motif clashes with the tsDNA in the aligned FnoCas12a complex. A multiple sequence alignment showed insertions of >10 amino acids in this region of YmeCas12a compared to homologs. Furthermore, this motif was enriched with polar side chains (Fig. 5B, bottom), indicating that it might interact with the nucleic acid substrate. We hypothesized that the longer motif in YmeCas12a could potentially inhibit *trans* substrate binding. We swapped the HLH motif of LbaCas12a (aa 82–98, purple in Fig. 5B, bottom panel) with YmeCas12a (aa 98–117, orange in Fig. 5B, bottom panel) based on the structural alignment to min-

imally interrupt the overall structure and named the chimera Yme^{HLH}.

The Yme^{HLH} construct maintained thermostability ([Supplementary Fig. S10a](#)) and exhibited ~2-fold higher *trans* activity relative to wild-type YmeCas12a regardless of the presence of dNTPs (Fig. 5C and [Supplementary Fig. S10b](#)). Curious if the mutation affected *cis* substrate cleavage, we determined the *cis*-cleavage kinetics. The *cis*-cleavage rates of the variant on either strand were very similar to that of wild-type YmeCas12a (Fig. 5D and [Supplementary Table S2](#)) and were not correlated with the changes in *trans* activities, consistent with our observation that the *cis* and *trans* activities were relatively uncoupled. We further measured the steady state kinetics of Yme^{HLH} and found that its improved *trans* activity was solely due to ~2-fold higher affinity to the *trans* substrate (2× lower K_m) without affecting k_{cat} (Fig. 5E and [Supplementary Table S3](#)). Altogether, these results demonstrated that engineering the unusually long HLH motif of YmeCas12a improved its *trans* nuclease activity without compromising nor relying on improving the *cis* activity.

Another HLH variant, derived from sequence alignment rather than structural alignments, did not show improvement over the wild-type YmeCas12a, even though the sequence was only two amino acids down shifted from the Yme^{HLH} design ([Supplementary Fig. S11a](#)). Further shortening of the HLH motif by removing an additional helix turn (or four amino acids) from Yme^{HLH}, did not enhance *trans* nuclease activity either ([Supplementary Fig. S11b](#)). We also explored other regions of YmeCas12a that showed obvious structural difference to LbaCas12a, but these variants were rendered mostly inactive ([Supplementary Fig. S12](#)).

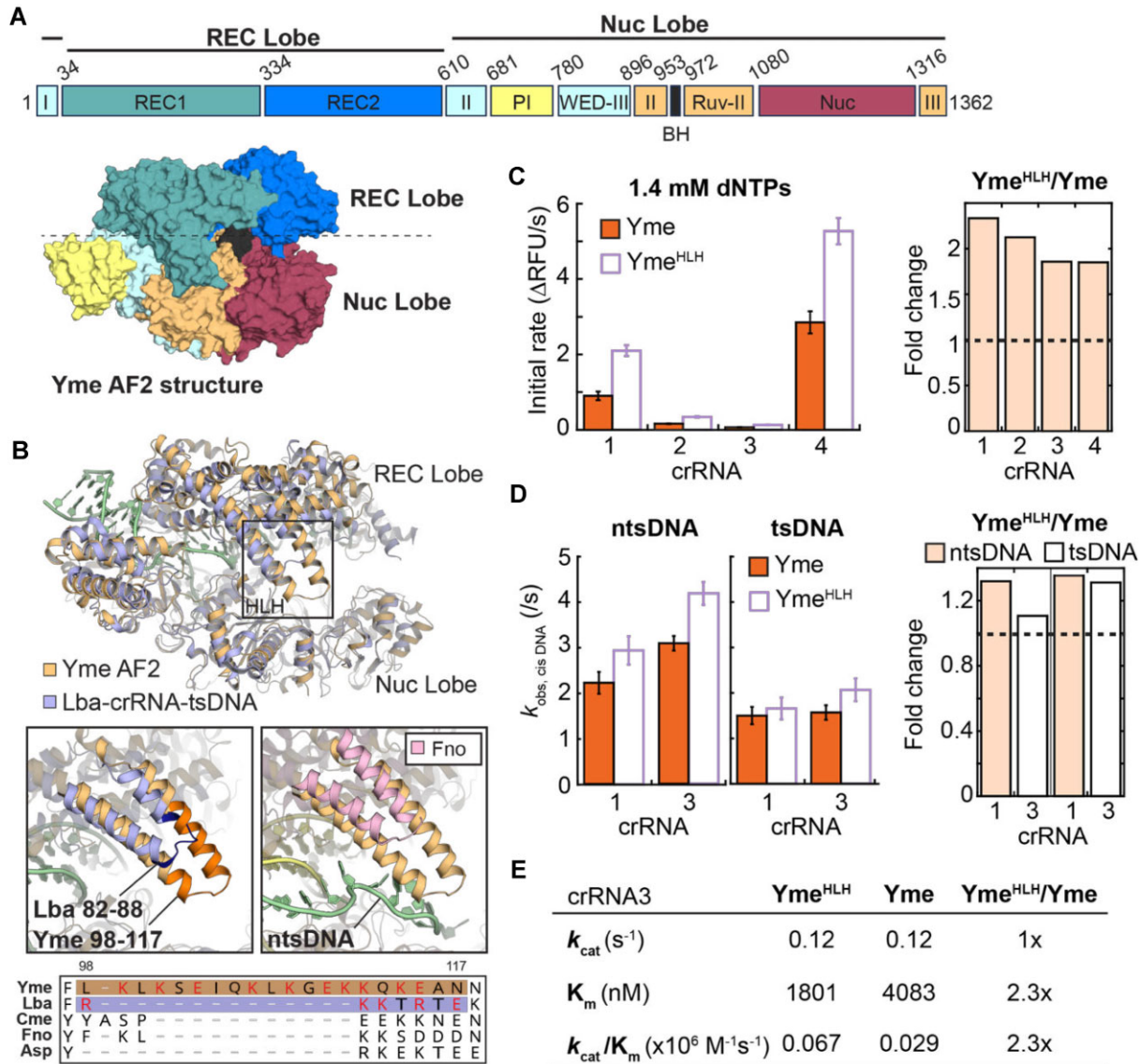


Figure 5. YmeCas12a *trans* activity improves by structure-guided helix-loop-helix tip swap. **(A)** YmeCas12a protein domain schematic and the predicted structure by AlphaFold 2 (AF2) with the same domain color code. The overall protein can be roughly divided into the REC and Nuc lobes. **(B)** Structural alignment of YmeCas12a with post-*cis* complex of LbaCas12a (PDB: 5XUS) or FnoCas12a (PDB: 6I1K). Insets of the REC lobe helix-loop-helix (HLH) tip illustrate the uniquely longer tip of YmeCas12a compared to orthologs (middle). Multiple sequence alignments of five Cas12a orthologs (bottom) shows the insertion in YmeCas12a. The YmeCas12a amino acids 98–117 (dark orange) were swapped with LbaCas12a amino acids 82–88 (dark purple) to generate variant Yme^{HLH}. The charged residues in this region are highlighted in red. **(C)** Initial *trans* cleavage rates of loop-swap variant Yme^{HLH} compared to YmeCas12a wild-type in the presence of 1.4 mM dNTPs. The fold change is shown on the right. **(D)** Reaction kinetics of Yme^{HLH} with the *cis* dsDNA substrate. The fold change is shown on the right. **(E)** Comparison of Michaelis-Menten kinetic parameters of Yme^{HLH} and YmeCas12a at the same target site (both with crRNA3). Parameters k_{cat} and K_m were averaged from at least 2 independent repeats.

YmeCas12a *trans* nuclease activity improves by introducing positively charged residues and fusion to DNA-binding protein

Nonspecific nuclease binding to DNA is mainly driven by electrostatic interactions [41]. Indeed, the ntsDNA binds to a positively charged groove on the surface of RuvC and Nuc domains in the LbaCas12a and FnoCas12a structures (Supplementary Fig. S13) [31]. We hypothesized that by introducing positively charged residues to the surface of RuvC and Nuc domains of YmeCas12a that face the ntsDNA, the *trans* substrate binding could be enhanced. We performed local alignments of the RuvC and Nuc domains of YmeCas12a and LbaCas12a (5XUS; RMSD_{C α} = 1.3Å) to analyze basic

side chain difference (Fig. 6A). The lysine (K) and arginine (R) residues either facing the ntsDNA or close to the active site that were present in LbaCas12a but absent in YmeCas12a were selected for mutagenesis. Five positions were mutated in Yme^{HLH} to the most conserved residue in a multiple sequence alignment or to the LbaCas12a equivalent (Fig. 6B) and the variants were assessed for *trans* cleavage activity (Fig. 6C). Among the variants, G1019K and I1155R each improved the *trans* nuclease activity ~2-fold, compared to parent enzyme Yme^{HLH} (Fig. 6C and Supplementary Fig. S14). Interestingly, the G1019K mutation is on the “lid region” that undergoes a loop-to-helix transition after *cis* substrate binding to unblock the nuclease active site pocket for catalysis [35, 36, 39]. The

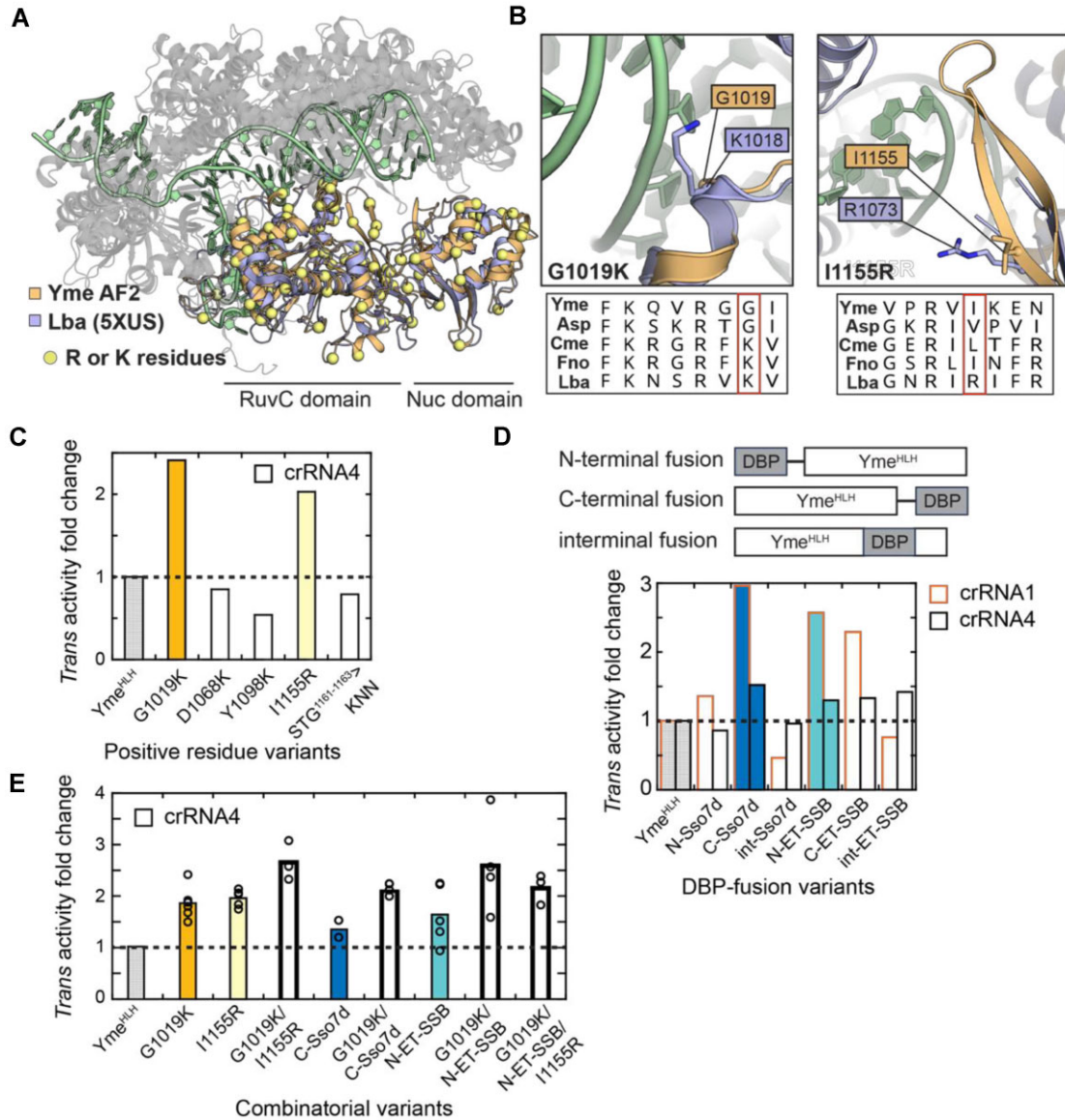


Figure 6. The Cas12a *trans* activity improves via structure-guided introduction of positively charged residue and fusion to DBP. **(A)** Local alignment of RuvC and Nuc domains of YmeCas12a and post-*cis* product complex of LbaCas12a (PDB: 5XUS). Alignment of the RuvC and Nuc domains, which bind and cleave the *trans* substrate, was performed to identify differences in arginine (R) and lysine (K) residues positions (α shown as yellow spheres) on the DNA-binding surface. **(B)** Example residue differences of YmeCas12a and LbaCas12a that were selected for site-directed mutagenesis. Sequence alignment of the five Cas12a orthologs were shown on the bottom with the changed residue framed in red. **(C)** Relative *trans* cleavage activity of the variants generated from introduction of positively charged residues. All variants were generated from Yme^{HLH}. **(D)** Schematic of the constructs of Yme^{HLH} fusion to a DBP is shown on the top. Fusion to the N- or C-terminus was designed with an X-Ten linker between the two proteins; the internal fusion was designed as direct insertion of a DBP to a predicted flexible loop without linkers. Representative results of the relative *trans* activity are shown as fold change relative to Yme^{HLH} on the bottom. **(E)** Relative *trans* activity of the combinatorial variants. The improved variants from panels (C) and (D), with the same color code, were combined to test the additive effect of the changes. Bars show the averaged *trans* activity from >3 repeats and results of each repeat are shown as circles. Variant Yme^{HLH}(G1019K/I1155R) was named as en-Yme for further tests.

introduced positive side chain could be poised to stabilize the *trans* substrate for cleavage.

Affinity to nucleic acids could also be improved by attaching a DBP to the target protein. Intriguingly, a recent study showed that fusion of RNA-binding protein to Cas13a improved Cas13a *trans* activity by improving affinity to its RNA *trans* substrate [42]. Thus, we designed N- and C-terminal DBP fusions to Yme^{HLH}, as well as an internal fusion in a flexible loop between the Nuc and RuvC domains (Fig. 6D, top). Because the NZ-GT reporter has a stem-loop structure, we tested both dsDNA (Sso7d) and ssDNA (ET-SSB) binding

proteins. Fusion of Sso7d to the C-terminus and fusion of ET-SSB to either of the C- or N-terminus improved *trans* nuclease activity in general (Fig. 6D and Supplementary Fig. S14). The effect of internal fusion, however, was variable and often detrimental. This is unsurprising as the internal fusion could easily disrupt the overall structure and render enzyme inactive or prevent substrate from accessing the active site. Even though further enhancement of *trans* nuclease activity may be achievable by testing additional DBPs and different linkers, these results confirm that fusion of DBP to Cas12a is an effective strategy in improving its *trans* nuclease activity.

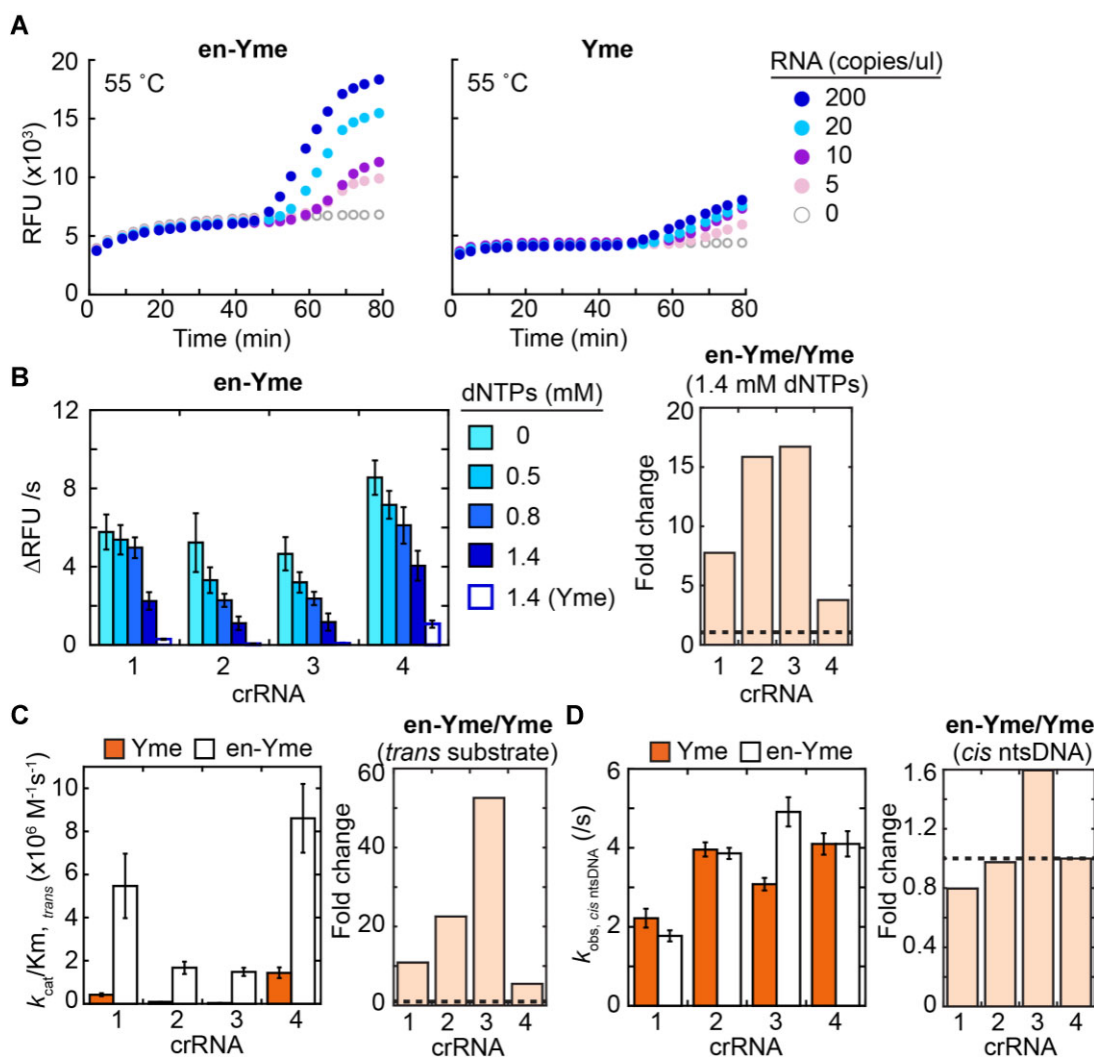


Figure 7. Characterization of en-Yme and its application in LAMP-Cas12a coupled one-pot diagnostics. **(A)** Performance of en-Yme in comparison to YmeCas12a wild-type in one-pot reactions coupling with RT-LAMP in detection of target RNA. Reactions were performed under the same condition with crRNA4. **(B)** Initial *trans* cleavage rates of en-Yme in the presence of dNTPs. Rates of YmeCas12a wild-type in the presence of 1.4 mM dNTPs (empty boxes) under the same condition are included for comparison. Relative rates of *trans* cleavage in the presence of 1.4 mM dNTPs are shown on the right. Dashed line indicates fold change of 1 (or no change). **(C)** Catalytic efficiency k_{cat}/K_m of en-Yme in comparison to YmeCas12a on the *trans* substrate. The parameters k_{cat} and K_m were averaged from at least two independent repeats. **(D)** Reaction kinetics of en-Yme in comparison to YmeCas12a with ntsDNA of the *cis* dsDNA substrate. Relative fold change of the ntsDNA cleavage rates is shown on the right.

Next, we tested whether combining these various strategies would have an additive effect in improving *trans* activity (Fig. 6E). The double combinatorial variants G1019K/I1155R, G1019K/C-Sso7d, and G1019K/N-ET-SSB each showed ~ 2 -fold higher *trans* activity compared to Yme^{HLH}. Adding I1155R to G1019K/N-ET-SSB to create the tri-partite variant G1019K/N-ET-SSB/I1155R did not yield further activity gains and instead caused protein instability during purification. Given its high *trans* activity and robust expression and purification, we selected G1019K/I1155R, hereafter engineered YmeCas12a (en-Yme), for further evaluation in one-pot nucleic acid detection.

Combinatorial variant en-Yme exhibits robust performance in one-pot reaction

Encouraged by the improved *trans* nuclease activity of en-Yme, we tested it in one-pot reactions with RT-LAMP for

RNA detection. Under identical conditions, en-Yme elicited a significantly stronger fluorescence response compared to wild-type YmeCas12a (Fig. 7A and Supplementary Fig. S15). Both enzymes detected RNA target as low as 5 copies/ μl , but en-Yme showed a much better signal-to-noise ratio. Interestingly, although Yme^{HLH} also exhibited increased *trans* activity, this did not translate into improved one-pot performance compared to the wild-type. Only en-Yme, with markedly higher *trans* activity, enhanced one-pot detection, highlighting the need for high *trans* activity to enable effective one-pot reactions.

To understand the underlying mechanism that contributed to better performance of en-Yme in LAMP-Cas one-pot reaction, we investigated the kinetics of this variant. Like YmeCas12, en-Yme *trans* nuclease activity was also inhibited by dNTPs in a dose-dependent manner (Fig. 7B, left). Despite the inhibition, the activity of en-Yme was 4- to 16-fold higher over that of YmeCas12a under the same condi-

tions (Fig. 7B, right). Similarly, en-Yme *trans* nuclease activity was less affected by the presence of NaCl (Supplementary Fig. S16a). Steady-state kinetic measurements with the *trans* substrate showed that en-Yme had a 5- to 52-fold higher specific activity (k_{cat}/K_m) than YmeCas12a, depending on the target site (Fig. 7C and Supplementary Table S3). Interestingly, the k_{cat} of en-Yme improved across the four targets (1.5- to 6-fold improvement over YmeCas12a), showing overall low target-dependent variation (1.1-fold maximum difference; Supplementary Table S3). Higher affinity to the *trans* substrate (K_m) was also observed across all four targets (4- to 8-fold). Therefore, the enhanced *trans* nuclease activity of en-Yme resulted from both higher catalytic activity and tighter binding to the *trans* substrate. We also observed that the *cis*-cleavage rate on either strand was very similar to that of YmeCas12a (0.8- to 1.6-fold difference for ntsDNA, Fig. 7D; 0.4- to 1.2-fold difference for tsDNA, Supplementary Fig. S16b), and were not correlated with the changes in *trans* kinetics.

Compared to wild-type, en-Yme showed improved *trans* nuclease activity in the presence of 1.4 mM dNTPs across all four targets, where the *trans* activity was comparable or higher relative to YmeCas12a with its best guide, crRNA4. Since crRNA4 was the only guide that showed sufficient *trans* activity to enable YmeCas12a in LAMP-Cas one-pot nucleic acid detection (Supplementary Fig. S3), we tested en-Yme with the other three guides. However, under the same reaction conditions, only crRNA4 supported specific detection of the target (Supplementary Fig. S17). These results highlight the complex nature of one-pot reactions, where the two competing reactions must be carefully balanced. They also underscore the importance of guide selection in development of one-pot diagnostics [6, 7].

In summary, by combining multiple strategies, we have engineered an efficient variant of thermostable Cas12a that enables robust one-pot LAMP-Cas nucleic acid detection. Compared to wild-type, en-Yme exhibits higher *trans* nuclease activity across all tested targeting sites, improved tolerance to salt and dNTPs, while maintaining its *cis* activity.

To evaluate whether the improved performance of en-Yme in the LAMP-Cas12a on-pot assay is broadly applicable, we extended our test to mpox, a DNA virus (Supplementary Fig. S18) [43]. Consistently, the en-Yme-based test yielded a markedly stronger signal than Yme-Cas12a under identical conditions and achieved a tenfold improvement in sensitivity, with a detection limit 200 copies/ μl compared to 2000 copies/ μl (Supplementary Fig. S18). These findings indicate that the enhanced activity of en-Yme is not restricted to specific targets or guide RNAs, but is broadly effective for nucleic acid detection, underscoring the generalizability of our mechanism- and structure-guided engineering approach.

Conclusion

LAMP is widely used for fast, simple, and sensitive nucleic acid detection in point-of-care (POC) settings. By coupling LAMP with Cas12a, detection specificity and sequence discrimination for SNPs and variant calling can be improved [15, 17, 44]. For POC nucleic acid detection, user-friendly one-pot assays that minimize cross-contamination and simplify test workflows are essential. To develop a robust LAMP-Cas12a one-pot molecular diagnostics assay, we engineered the thermostable YmeCas12a for enhanced *trans* nuclease activity.

The optimized enzyme demonstrates improved *trans* nuclease activity across all tested target sites and significantly boosts signal in LAMP-Cas12a one-pot reaction. Its enhanced nuclease activity and thermostability allow it to be directly integrated into the LAMP workflow, operating at a temperature lower than LAMP's optimal but effectively balancing both reactions, ensuring neither is compromised and no extra steps are needed.

Cas12a nucleases uses a RuvC nuclease domain for both *cis* and *trans* DNA cleavage, but understanding of the regulation and interplay between these activities remained incomplete. Our kinetic resolution of the two steps fills in this gap and suggests that *cis* and *trans* DNA cleavage steps are relatively uncoupled, consistent with previous studies indicating that RuvC resets after each round of *cis* reaction (ntsDNA then tsDNA) [35, 36]. The observed kinetic difference in each step is likely caused by the large conformational rearrangements that Cas12a enzyme undertakes between the *cis* and *trans* reactions [3, 36, 45–47], which influence both substrate binding and phosphodiester bond scission efficiency. Rather than the previously considered diffusion-limited reaction [4], the *trans* nuclease activity has been found to be far less efficient [48]. In agreement, our kinetic study reveals that poor *trans* substrate binding is the key limiting factor in Cas12a *trans* activity. It is important to point out that the observed kinetics for *cis* and *trans* reactions measured here are not a direct readout of catalytic rates, but the combination of multiple steps for each reaction. The kinetic rates therefore represent a lower limit of activating the RuvC active site for *cis* or *trans* substrate cleavage. Nonetheless, our kinetic study performed here provides important guidelines to engineer Cas12a for efficient *trans* nuclease activity.

One-pot reactions that couple amplification and Cas nuclease activity must balance these two interdependent yet mutually inhibitory processes. Cas12a relies on the accumulation of LAMP product (*cis* substrate) for activation of *trans* nuclease activity, but activated Cas12a can cleave the LAMP product, both in *cis* and in *trans*, which in turn inhibits amplification. On the other hand, high dNTPs concentrations required by LAMP inhibit Cas12a *trans* activity, and the DNA polymerase in LAMP reactions could dislodge Cas12a from the *cis* substrate, deactivating Cas12a. Consistent with this, a recent study showed that lower RNP concentrations, counterintuitively, improved the sensitivity in one-pot reactions coupling recombinase-aided amplification (RAA) and Cas12a [49]. Similarly, efficient one-pot reaction coupling recombinase polymerase amplification (RPA) and Cas12a was demonstrated by using suboptimal PAMs [50], on the basis that suboptimal PAMs slow down Cas12a reaction to favor amplification at early stage thus generating enough amplicon for detection. Our results with the en-Yme variant in LAMP-Cas12a one-pot reactions (Fig. 7A and Supplementary Fig. S17) also suggest that while high *trans* activity is essential, it is not enough for successful one-pot detection. Therefore, improvement of the Cas *trans* nuclease activity is best performed early in the one-pot assay development. Once the *trans* nucleases activity meets a critical threshold, a sensitive and efficient one-pot reaction requires balanced kinetics of the two competing reactions, which could be achieved empirically by optimization of conditions like RNP concentration, temperature, and additives [7, 17, 20, 51].

In conclusion, we demonstrate a framework for engineering highly efficient Cas12a enzymes by combining kinetic stud-

ies of its *cis* and *trans* nuclease activities with integrative enzyme engineering approaches. These strategies are potentially applicable to other Cas nucleases, both to better understand the reaction mechanisms and regulation, and to enhance their *trans* nuclease activity for specific applications. Additionally, our findings lay the groundwork for future development of multiplexed isothermal nucleic acid detection, such as in combination with thermostable Cas12b and Cas13a.

Acknowledgements

We thank Robert Trachman for his help with Cas12a structural analysis. Yinhu Zhang for his discussion on LAMP reaction mechanism. We are also grateful for insightful discussions from the NEB community, with special thanks to Joe Whipple, Ira Schildkraut, and Zach Carter for discussions and critical comments on the manuscript.

Author contributions: Juan Pan: conceptualization, investigation, formal analysis, methodology, project administration, visualization, and writing of the draft. Megumu Mabuchi: data curation and formal analysis. Daniel W. Kneller: visualization. Ryan T. Fuchs, Jennifer L. Curcuru, Esta Tamanaha, and Nathan A. Tanner: formal analysis. G. Brett Robb and Ivan R. Corrêa Jr.: supervision and resources. All authors reviewed the manuscript.

Supplementary data

Supplementary data is available at NAR online.

Conflict of interest

The authors are current or previous employees in the Research Department of New England Biolabs, Inc. (NEB). NEB is a commercial supplier of molecular biology reagents, including some that were used in this work.

Funding

New England Biolabs, Inc. Funding to pay the Open Access publication charges for this article was provided by New England Biolabs, Inc.

Data availability

The data underlying this article are available in the article and in its online supplementary material.

References

- Yan WX, Hunnewell P, Alfonse LE *et al.* Functionally diverse type V CRISPR–Cas systems. *Science* 2019;363:88–91. <https://doi.org/10.1126/science.aav7271>
- Makarova KS, Wolf YI, Alkhnbashi OS *et al.* An updated evolutionary classification of CRISPR–Cas systems. *Nat Rev Micro* 2015;13:722–36. <https://doi.org/10.1038/nrmicro3569>
- Li S-Y, Cheng Q-X, Liu J-K *et al.* CRISPR–Cas12a has both *cis*- and *trans*-cleavage activities on single-stranded DNA. *Cell Res* 2018;28:491–3. <https://doi.org/10.1038/s41422-018-0022-x>
- Chen JS, Ma E, Harrington LB *et al.* CRISPR–Cas12a target binding unleashes indiscriminate single-stranded DNase activity. *Science* 2018;360:436–9. <https://doi.org/10.1126/science.aar6245>
- Broughton JP, Deng X, Yu G *et al.* CRISPR–Cas12-based detection of SARS-CoV-2. *Nat Biotechnol* 2020;38:870–4. <https://doi.org/10.1038/s41587-020-0513-4>
- Li L, Li S, Wu N *et al.* HOLMESv2: a CRISPR–Cas12b-assisted platform for nucleic acid detection and DNA methylation quantitation. *ACS Synth Biol* 2019;8:2228–37. <https://doi.org/10.1021/acssynbio.9b00209>
- Joung J, Ladha A, Saito M *et al.* Detection of SARS-CoV-2 with SHERLOCK one-pot testing. *N Engl J Med* 2020;383:1492–4. <https://doi.org/10.1056/NEJMc2026172>
- Li X, Dang Z, Tang W *et al.* Detection of parasites in the field: the ever-innovating CRISPR/Cas12a. *Biosensors* 2024;14:145. <https://doi.org/10.3390/bios14030145>
- Glöckler J, Lim TS, Ida J *et al.* Isothermal amplifications—a comprehensive review on current methods. *Crit Rev Biochem Mol Biol* 2021;56:543–86. <https://doi.org/10.1080/10409238.2021.1937927>
- Notomi T, Okayama H, Masubuchi H *et al.* Loop-mediated isothermal amplification of DNA. *Nucleic Acids Res* 2000;28:63e–63. <https://doi.org/10.1093/nar/28.12.e63>
- Plutzer J, Karanis P. Rapid identification of *Giardia duodenalis* by loop-mediated isothermal amplification (LAMP) from faecal and environmental samples and comparative findings by PCR and real-time PCR methods. *Parasitol Res* 2009;104:1527–33. <https://doi.org/10.1007/s00436-009-1391-3>
- Zhang Y, Odiwuor N, Xiong J *et al.* Rapid molecular detection of SARS-CoV-2 (COVID-19) virus RNA using colorimetric LAMP. medRxiv, <https://doi.org/10.1101/2020.02.26.20028373>, 29 February 2020, preprint: not peer reviewed.
- Katsanis SH, Katsanis N. Molecular genetic testing and the future of clinical genomics. *Nat Rev Genet* 2013;14:415–26. <https://doi.org/10.1038/nrg3493>
- Land KJ, Boeras DI, Chen X-S *et al.* REASSURED diagnostics to inform disease control strategies, strengthen health systems and improve patient outcomes. *Nat Microbiol* 2019;4:46–54. <https://doi.org/10.1038/s41564-018-0295-3>
- Kaminski MM, Abudayyeh OO, Gootenberg JS *et al.* CRISPR-based diagnostics. *Nat Biomed Eng* 2021;5:643–56. <https://doi.org/10.1038/s41551-021-00760-7>
- Trung NT, Son LHP, Hien TX *et al.* CRISPR–Cas12a combination to alleviate the false-positive in loop-mediated isothermal amplification-based diagnosis of *Neisseria meningitidis*. *BMC Infect Dis* 2022;22:429. <https://doi.org/10.1186/s12879-022-07363-w>
- Pang B, Xu J, Liu Y *et al.* Isothermal amplification and ambient visualization in a single tube for the detection of SARS-CoV-2 using loop-mediated amplification and CRISPR technology. *Anal Chem* 2020;92:16204–12. <https://doi.org/10.1021/acs.analchem.0c04047>
- Figueiredo D, Cascalheira A, Goncalves J. Rapid, multiplex detection of SARS-CoV-2 using isothermal amplification coupled with CRISPR–Cas12a. *Sci Rep* 2023;13:849. <https://doi.org/10.1038/s41598-022-27133-7>
- Yang T, Chen Y, He J *et al.* A designed vessel using dissolvable polyvinyl alcohol membrane as automatic valve to couple LAMP with CRISPR–Cas12a system for visual detection. *Biosensors* 2023;13:111. <https://doi.org/10.3390/bios13010111>
- Ding X, Yin K, Li Z *et al.* Sensitive quantitative detection of SARS-CoV-2 in clinical samples using digital warm-start CRISPR assay. *Biosens Bioelectron* 2021;184:113218. <https://doi.org/10.1016/j.bios.2021.113218>
- Pudziulevytė I, Olechnovič K, Godliauskaitė E *et al.* TemStaPro: protein thermostability prediction using sequence representations from protein language models. *Bioinformatics* 2024;40:btac157. <https://doi.org/10.1093/bioinformatics/btac157>
- Fuchs RT, Curcuru JL, Mabuchi M *et al.* Characterization of Cme and Yme thermostable Cas12a orthologs. *Commun Biol* 2022;5:325. <https://doi.org/10.1038/s42003-022-03275-2>

23. Singh D, Mallon J, Poddar A *et al.* Real-time observation of DNA target interrogation and product release by the RNA-guided endonuclease CRISPR Cpf1 (Cas12a). *Proc Natl Acad Sci USA* 2018;115:5444–9. <https://doi.org/10.1073/pnas.1718686115>
24. Zetsche B, Gootenberg JS, Abudayyeh OO *et al.* Cpf1 is a single RNA-guided endonuclease of a Class 2 CRISPR–Cas system. *Cell* 2015;163:759–71. <https://doi.org/10.1016/j.cell.2015.09.038>
25. Pan J, Mabuchi M, Robb GB. DNA rehybridization drives product release from Cas9 ribonucleoprotein to enable multiple-turnover cleavage. *Nucleic Acids Res* 2023;51:3903–17. <https://doi.org/10.1093/nar/gkad233>
26. Gong S, Yu HH, Johnson KA *et al.* DNA unwinding is the primary determinant of CRISPR–Cas9 activity. *Cell Rep* 2018;22:359–71. <https://doi.org/10.1016/j.celrep.2017.12.041>
27. Greenough L, Schermerhorn KM, Mazzola L *et al.* Adapting capillary gel electrophoresis as a sensitive, high-throughput method to accelerate characterization of nucleic acid metabolic enzymes. *Nucleic Acids Res* 2016;44:e15. <https://doi.org/10.1093/nar/gkv899>
28. Mirdita M, Schütze K, Moriwaki Y *et al.* ColabFold: making protein folding accessible to all. *Nat Methods* 2022;19:679–82. <https://doi.org/10.1038/s41592-022-01488-1>
29. Jumper J, Evans R, Pritzel A *et al.* Highly accurate protein structure prediction with AlphaFold. *Nature* 2021;596:583–9. <https://doi.org/10.1038/s41586-021-03819-2>
30. Yamano T, Zetsche B, Ishitani R *et al.* Structural basis for the canonical and non-canonical PAM recognition by CRISPR–Cpf1. *Mol Cell* 2017;67:633–45. <https://doi.org/10.1016/j.molcel.2017.06.035>
31. Swarts DC, Jinek M. Mechanistic insights into the *cis*- and *trans*-acting DNase activities of Cas12a. *Mol Cell* 2019;73:589–600. <https://doi.org/10.1016/j.molcel.2018.11.021>
32. Qi LS, Larson MH, Gilbert LA *et al.* Repurposing CRISPR as an RNA-guided platform for sequence-specific control of gene expression. *Cell* 2013;152:1173–83. <https://doi.org/10.1016/j.cell.2013.02.022>
33. Zhang Y, Ren G, Buss J *et al.* Enhancing colorimetric loop-mediated isothermal amplification speed and sensitivity with guanidine chloride. *BioTechniques* 2020;69:178–85. <https://doi.org/10.2144/btn-2020-0078>
34. Swarts DC. Making the cut(s): how Cas12a cleaves target and non-target DNA. *Biochem Soc Trans* 2019;47:1499–510. <https://doi.org/10.1042/BST20190564>
35. Saha A, Ahsan M, Arantes PR *et al.* An alpha-helical lid guides the target DNA toward catalysis in CRISPR–Cas12a. *Nat Commun* 2024;15:1473. <https://doi.org/10.1038/s41467-024-45762-6>
36. Stella S, Mesa P, Thomsen J *et al.* Conformational activation promotes CRISPR–Cas12a catalysis and resetting of the endonuclease activity. *Cell* 2018;175:1856–71. <https://doi.org/10.1016/j.cell.2018.10.045>
37. Swarts DC, Oost Jvd, Jinek M. Structural basis for guide RNA processing and seed-dependent DNA targeting by CRISPR–Cas12a. *Mol Cell* 2017;66:221–33. <https://doi.org/10.1016/j.molcel.2017.03.016>
38. Stella S, Alcón P, Montoya G. Structure of the Cpf1 endonuclease R-loop complex after target DNA cleavage. *Nature* 2017;546:559–63. <https://doi.org/10.1038/nature22398>
39. Strohkendl I, Saha A, Moy C *et al.* Cas12a domain flexibility guides R-loop formation and forces RuvC resetting. *Mol Cell* 2024;84:2717–31. <https://doi.org/10.1016/j.molcel.2024.06.007>
40. Drummond RSM. Cas12 detection methods and compositions. WO 2022/118200 A1. 2022.
41. von Hippel PH. From “simple” DNA–protein interactions to the macromolecular machines of gene expression. *Annu Rev Biophys Biomol Struct* 2007;36:79–105. <https://doi.org/10.1146/annurev.biophys.34.040204.144521>
42. Yang J, Song Y, Deng X *et al.* Engineered LwaCas13a with enhanced collateral activity for nucleic acid detection. *Nat Chem Biol* 2023;19:45–54. <https://doi.org/10.1038/s41589-022-01135-y>
43. Li Z, Sinha A, Zhang Y *et al.* Extraction-free LAMP assays for generic detection of Old World Orthopoxviruses and specific detection of Mpox virus. *Sci Rep* 2023;13:21093. <https://doi.org/10.1038/s41598-023-48391-z>
44. Fasching CL, Servellita V, McKay B *et al.* COVID-19 variant detection with a high-fidelity CRISPR–Cas12 enzyme. *J Clin Microbiol* 2022;60:e00261-22. <https://doi.org/10.1128/jcm.00261-22>
45. Wörle E, Jakob L, Schmidbauer A *et al.* Decoupling the bridge helix of Cas12a results in a reduced trimming activity, increased mismatch sensitivity and impaired conformational transitions. *Nucleic Acids Res* 2021;49:5278–93. <https://doi.org/10.1093/nar/gkab286>
46. Zhang F, Huang Z. Mechanistic insights into the versatile class II CRISPR toolbox. *Trends Biochem Sci* 2022;47:433–50. <https://doi.org/10.1016/j.tibs.2021.11.007>
47. Saha A, Arantes PR, Hsu RV *et al.* Molecular dynamics reveals a DNA-induced dynamic switch triggering activation of CRISPR–Cas12a. *J Chem Inf Model* 2020;60:6427–37. <https://doi.org/10.1021/acs.jcim.0c00929>
48. Ramachandran A, Santiago JG. CRISPR enzyme kinetics for molecular diagnostics. *Anal Chem* 2021;93:7456–64. <https://doi.org/10.1021/acs.analchem.1c00525>
49. Chen Y, Mei Y, Zhao X *et al.* Reagents-loaded, automated assay that integrates recombinase-aided amplification and Cas12a nucleic acid detection for a point-of-care test. *Anal Chem* 2020;92:14846–52. <https://doi.org/10.1021/acs.analchem.0c03883>
50. Lu S, Tong X, Han Y *et al.* Fast and sensitive detection of SARS-CoV-2 RNA using suboptimal protospacer adjacent motifs for Cas12a. *Nat Biomed Eng* 2022;6:286–97. <https://doi.org/10.1038/s41551-022-00861-x>
51. Aman R, Marsic T, Rao GS *et al.* iSCAN-V2: a one-pot RT-RPA-CRISPR–Cas12b assay for point-of-care SARS-CoV-2 detection. *Front Bioeng Biotechnol* 2021;9:800104. <https://doi.org/10.3389/fbioe.2021.800104>